Biomicrofluidics ARTICLE scitation.org/journal/bmf

Cancer cell migration and cancer drug screening in oxygen tension gradient chip

Cite as: Biomicrofluidics 14, 044107 (2020); doi: 10.1063/5.0011216
Submitted: 21 April 2020 · Accepted: 28 June 2020 ·
Published Online: 21 July 2020

View Online Export Citation CrossMark

Hyeono Nam,[1] Kenichi Funamoto,[2,3,a)] and Jessie S. Jeon[1,4,a)]

AFFILIATIONS

[1]Department of Mechanical Engineering, Korea Advanced Institute of Science and Technology, Daejeon 34141, South Korea
[2]Institute of Fluid Science, Tohoku University, Sendai 980-8577, Japan
[3]Graduate School of Engineering, Tohoku University, Sendai, 980-8579, Japan
[4]KAIST Institute for Health Science and Technology, Korea Advanced Institute of Science and Technology, Daejeon 34141, South Korea

[a)]**Authors to whom correspondence should be addressed:** funamoto@tohoku.ac.jp and jsjeon@kaist.ac.kr

ABSTRACT

Cancer metastasis, which is prevalent in malignant tumors, is present in a variety of cases depending on the primary tumor and metastatic site. The cancer metastasis is affected by various factors that surround and constitute a tumor microenvironment. One of the several factors, oxygen tension, can affect cancer cells and induce changes in many ways, including motility, directionality, and viability. In particular, the oxygen tension gradient is formed within a tumor cluster and oxygen is lower toward the center of the cluster from the perivascular area. The simple and efficient designing of the tumor microenvironment using microfluidic devices enables the simplified and robust platform of the complex *in vivo* microenvironment while observing a clear cause-and-effect between the properties of cancer cells under oxygen tension. Here, a microfluidic device with five channels including a gel channel, media channels, and gas channels is designed. MDA-MB-231cells are seeded in the microfluidic device with hydrogel to simulate their three-dimensional movement in the body. The motility and directionality of the cancer cells under the normoxic and oxygen tension gradient conditions are compared. Also, the viability of the cancer cells is analyzed for each condition when anticancer drugs are applied. Unlike the normoxic condition, under the oxygen tension gradient, cancer cells showed directionality toward higher oxygen tension and decreased viability against the certain anticancer drug. The simplified design of the tumor microenvironment through microfluidic devices enables comprehension of the response of cancer cells to varying oxygen tensions and cancer drugs in the hypoxic tumor microenvironment.

I. INTRODUCTION

Cancer metastasis refers to the spread of a tumor from the primary site to the secondary sites within the body. The risk of cancer metastasis from malignant tumors is emphasized because of the possibility of secondary tumor formation at the target organ which leads to the increased mortality. In particular, breast cancer, which is most common among women, is highly metastatic.[1] Therefore, early treatment is important to prevent the secondary tumor formation, and consequently, the market for the cancer treatment is also growing.[2,3]

In the tumor microenvironment, cancer cells are usually clustered in the form of spheroids and affect the extracellular matrix (ECM), the vascular system, the lymphatic system, and various cell types (lymphocytes, macrophages, fibroblasts, neutrophils) around that milieu.[4,5] These excessive tumor mass in a confined space makes a reduced supply of various nutrients for survival, including oxygen, relative to the normal tissue.[6] The tumor microenvironment with poor oxygen supply leads to chronic or transient hypoxia, which changes the characteristics and the physiologies of the cancer cells including motility and drug resistance through oxygen-specific marker, hypoxia-inducible factor (HIF).[7,8] Changes in the motility of cancer cells by the HIF pathway can be found not only in the constant hypoxic environment but also in the periodic hypoxic environment.[9]

Recently, some studies on the motility of cancer cells under the hypoxic environment have been conducted, and they revealed that the hypoxic environment affects the activity of the cancer cells.[10,11] Therefore, when it comes to the cancer metastasis, the hypoxic environment is a valuable area of discussion. Besides the

cancer cell motility, the efficacy of anticancer drugs could also be different in the conditions of hypoxia and normoxia.[6] Due to hypoxic conditions, certain anticancer drugs are known to enhance their efficacy in a hypoxic environment.[12,13] Thus, the study of the hypoxic tumor microenvironment is essential for understanding the tumor model as well as when screening for anticancer drugs.

However, it is difficult to observe the distinct causality of cancer cell behaviors and hypoxic stimulation *in vivo* because of simultaneous action of the various physicochemical factors including blood flow[14] and different kinds of chemoattractants.[15,16] These multiple factors affect the characteristics and physiologies of the cancer cells in addition to the formation of the hypoxic condition in the tumor microenvironment.[17] As an example, *in vivo* experiments with xenograft models require a transplantation between different animals, which means that some genetic defects and the lack of an immune response make it difficult to achieve the corresponding efficient results.[18] On the other hand, *in vitro* experiments have the advantages of cost-effectiveness and high throughput compared to the *in vivo* experiments, but the conventional two-dimensional (2D) *in vitro* experiments are insufficient to simulate the physiological environment in the body. Understandably, in three-dimensional (3D) microenvironment, cells exhibit different morphological and mechanical behaviors than in the 2D environment.[19] Furthermore, cell culture conditions are crucial to the cellular behavior that depending on the cell culture condition, even at the same drug concentration, some anticancer drugs may selectively develop a drug resistance.[20] Microfluidic-based 3D *in vitro* experimental systems have emerged to overcome this problem and have the advantage in mimicking physiological microenvironment.[21] In addition, the hydrodynamically designed devices allow us to investigate on cellular behaviors by controlling concentration of chemoattractants, flow rate, and various physical stimuli that were difficult to control with *in vivo* experiments.[22] In these regards, the microfluidic devices not only enable the simulation of 3D microenvironments in the body but also allow comparisons on the migratory behavior as well as the drug response of cancer cells in hypoxic environments.

Indeed, the oxygen tension varies between organs within the body, and a number of previous studies worked on controlling oxygen tension in microfluidic devices. Since polydimethylsiloxane (PDMS), a porous material, has permeable properties to gas, there have been attempts to control the peripheral area of the device with diffusion by designing a separate gas channel in the microfluidic device.[23–25] Using this technique, the previous research analyzed the signaling pathways and the physical behavior of the cells related to the hypoxic environment by controlling the oxygen tension in the microfluidic devices.[26,27] These studies on the physical properties of cells have focused on the homogeneous low oxygen levels in the body and applied constant low oxygen tension environment. However, in the actual tumor microenvironment, the oxygen tension decreases toward the center of the tumor, forming an oxygen tension gradient, and thus, an additional study is required.[28]

Here, we present a microfluidic device with an oxygen tension gradient to mimic the oxygen tension gradient produced in a tumor microenvironment. Fine control of oxygen level allows us to observe the delicate responses of cells to the external stimuli. We form a stable oxygen tension gradient in the microfluidic device and show that the cancer cells tend to migrate in the direction of higher oxygen tension in the region where the oxygen tension gradient is formed. Furthermore, in the case of certain anticancer drugs, the oxygen-dependent efficacy is observed. The microfluidic device, which is designed to consider the oxygen gradient in tumor microenvironment, makes it possible to more clearly observe the causal relationship between the changes in the oxygen tension and the responses of the cancer cells that were difficult to observe previously. Therefore, these results contribute in further development of *in vitro* models for future studies on tumor microenvironment and cancer treatments.

II. MATERIALS AND METHODS

A. Microfluidic system

A microfluidic device composed of five channels including a gel channel, media channels, and gas channels was designed by

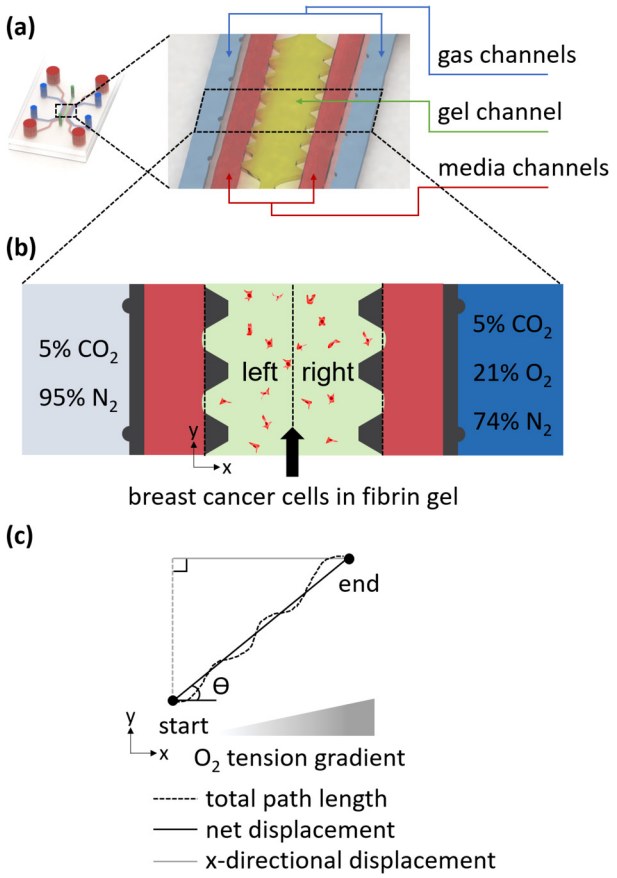

FIG. 1. Schematic of the microfluidic system. (a) The microfluidic device consists of two gas channels (blue), one gel channel (lime green), and two media channels (red). (b) Schematic under the condition of oxygen tension gradient. Oxygen-permeable PDMS yields gas exchange between gas channels (light blue and blue) and the middle gel channel (lime green), where cancer cells (red dots) are present. The migration of the cancer cells was analyzed by dividing the oxygen tension into a low level (left) and a high level (right). (c) Definition of migration metrics.

referring to the previous research [Fig. 1(a)].[26,29] The gas channels are arranged symmetrically about the gel channel. Each gas channel is spaced 150 μm from the medium channels adjacent to the gel channel. Since PDMS is gas-permeable, the intermediate gel and medium channels are thus affected by gases with different oxygen tensions that diffuse from the gas channels. A single-layered SU-8 mold with the device design was made by the negative photoresist. Briefly, a mixture of polydimethylsiloxane (PDMS, Dow Corning) base and the curing agent at a weight ratio of 10:1 was poured on the mold. Then, the bubbles encapsulated in the mold were removed by placing it in a vacuum desiccator. After curing for 2 h in an oven at 80 °C, the ports of gel channel, gas channels, and media channels were punched using a puncher having a diameter of 1, 2, and 4 mm, respectively. Perforated PDMS was sterilized in the autoclave with and without de-ionized water (DI water). Finally, the PDMS and a coverslip sterilized by the same procedure were bonded after plasma treatment and incubated in the oven overnight for recovery of hydrophobicity.

B. Cell culture

MDA-MB-231 cells (Korean Cell Line Bank) were cultured in Dulbecco's modified Eagle's medium (DMEM, Lonza) supplemented with 10% (v/v) fetal bovine serum (FBS, Gibco) and 1% (v/v) antibiotic-antimycotic solution (Gibco). The cells were incubated in a CO_2 incubator at 37 °C and 5% CO_2. When the cancer cells reached 70–80 confluency, 0.25% trypsin-EDTA (Gibco) was used to detach the cancer cells from the culture dish. The detached cancer cells were concentrated to 0.6×10^6 cells/ml in 4 U/ml thrombin solution. Next, a fibrin gel at the final concentration of 2.5 mg/ml with a cell density of 0.3×10^6 cells/ml was injected into the gel channel by mixing a 1:1 volumetric ratio of 5 mg/ml fibrinogen solution and the previous thrombin solution containing cell suspension [Fig. 1(b)]. The gel-infused device was placed in the humidity chamber for 12 min for gelation and incubated for one day before each experiment for the mechanical stabilization of the gel.

C. Generation of oxygen tension gradient and validation

Oxygen tension gradient was formed in the cell culture region of the microfluidic device by flowing anoxic gas in the right gas channel and normoxic gas in the left gas channel. The anoxic gas consisted of 0% O_2, 5% CO_2, and 95% N_2, whereas the normoxic gas mixture contained 21% O_2, 5% CO_2, and 74% N_2 [Fig. 1(b)].

Two methods, simulation and experimental approaches, were used to check the oxygen tension in the microfluidic device. First, commercial finite element software (COMSOL Multiphysics 5.3a, COMSOL Inc.) was used for the simulation. The continuity equation, the Navier–Stokes equations, and the convection–diffusion equation were employed for the gas flow analysis and calculation of the oxygen tension in the microfluidic device. The properties (density, viscosity, diffusivity, etc.) of gel, medium, PDMS, and gas for the numerical analysis were referred by the previous study.[26] And the Péclet number, a dimensionless number, was used to investigate the convection and diffusion of the oxygen in the device according to the gas flow rate,

$$Pe = \frac{UL}{D}, \tag{1}$$

where U is the average flow velocity in the gas channels, L is the hydraulic diameter of the gas channels, and D is diffusivity of oxygen in the air. The contents of the simulation are divided into three parts. First, the oxygen tension in the gel and media channels was calculated according to the magnitude of the Pe number at steady-state [Figs. S1(a) and S1(b) in the supplementary material]. Next, when the Pe number was 100, the oxygen tension of the gel channel was calculated in the transient state [Figs. S1(c) and S1(d) in the supplementary material]. Finally, the oxygen tension at the center of the gel channel was represented by a convergence curve over time [Fig. 2(a)].

As an experimental approach to verify the simulation results, the oxygen-sensitive dye tris(2,2′-bipyridyl) dichlororuthenium (II) hexahydrate (RTDP, Sigma-Aldrich) was used. RTDP at 5 mg/ml was filled in the gel and medium channels of the device. In order

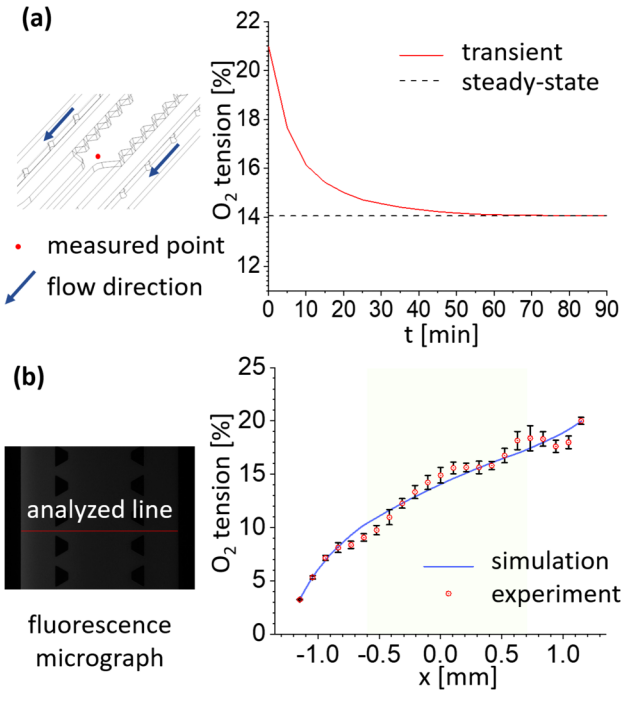

FIG. 2. Oxygen tension validation through simulation and experimental methods confirms that the oxygen tension gradient forms stably. (a) The convergence curve of the oxygen tension at the midpoint of the gel channel (red dot) was calculated. The gas flow velocity was set to $Pe = 100$. In the graph, the oxygen tension changed significantly until 30 min and then reached a quasi-steady-state after 60 min. (b) Fluorescence images from the oxygen-sensitive dye were analyzed in the direction across the channel as shown. The graph shows the oxygen tension gradient formed in the gel channel (lime green) as a result of the experiment and simulation when $Pe = 100$. Error bars mean the standard deviation.

to measure the oxygen tension at the steady-state, a fluorescent image was measured 90 min after the gas was supplied to the gas channels (Fig. S2 in the supplementary material). A sufficient flow rate of gas was flowed to prevent changes in gas composition inside the gas channels. In order to remove the background noise caused by the fluorescence refraction generated by the microstructure of the device, the gray value of the reference fluorescent image, which was taken before the gas flows, was subtracted from image under the oxygen tension gradient using ImageJ (Fig. S2 in the supplementary material). Then, the oxygen tension was calculated from the corrected gray values by applying the Stern–Volmer equation.[30] To confirm the uniformity of the oxygen tension inside the device, fluorescent intensities at five different locations between five pairs of seven microposts were analyzed and averaged.

D. Cellular experiment under controlled oxygen tension

The experiment for the characterization of the cellular oxygen tension was conducted under three conditions in a microfluidic device with 3D microenvironment (Fig. S5 in the supplementary material). First, in the oxygen tension gradient, the gel channel was divided into two sections for checking the cellular responses according to the range of oxygen tension in detail [Fig. 1(b)]. Next, the cellular responses in normoxic conditions were observed as a comparative group. Finally, the responses with 100 μM $CoCl_2$, which generates uniform hypoxic condition, were examined as a positive control.[31]

E. Immunofluorescent staining

The media in the reservoirs of the media channels was removed by pipet and washed with phosphate buffered saline (PBS, Lonza). After fixation of 20 min at room temperature using 4% paraformaldehyde (PFA), the samples were permeabilized for 30 min with 0.5% Triton X-100 solution. The solution was then removed from all reservoirs and washed twice with PBS. CAS-Block (Thermo Fisher Scientific) was treated at room temperature for 1 h, and then, HIF-1α was labeled with rabbit polyclonal antibody (Thermo Fisher Scientific) at 1:100 dilution was incubated overnight at 4 °C. After washing the channels five times with 0.1% bovine serum albumin (BSA) solution, Alexa Fluor 488 (Thermo Fisher Scientific), 4′,6-diamidino-2-phenylindole (DAPI, Thermo Fisher Scientific), and 0.1% BSA solution with the ratio of 5:1:1000 were added to the reservoirs. The incubation continued overnight at 4 °C. Finally, after washing three times with 0.1% BSA solution, fluorescence images were taken.

F. Motility and directionality characterization

To quantify the motility and directionality of the cancer cells, the oxygen tension gradient generated condition and the normoxic condition were compared. In order to enhance the cellular activity, a media with the concentration of 50 ng/ml human epidermal growth factor (hEGF, Sigma-Aldrich) was used.[16] For the stable formation of oxygen tension gradient, there was no flow in the medium channels. The gases were supplied to the gas channels for 8 h and the last 6 h (=T) were measured at 10-min intervals. The obtained 37 bright-field images were then concatenated, and the cancer cells were manually tracked for the measurement of net displacement (ND), total path length (TPL), and x-directional displacement (XDD) [Fig. 1(c)],

$$ND = \sqrt{(y_{37} - y_1)^2 + (x_{37} - x_1)^2}, \tag{2}$$

$$TPL = \sum_{i=1}^{36} \sqrt{(y_{i+1} - y_i)^2 + (x_{i+1} - x_i)^2}, \tag{3}$$

$$XDD = x_{37} - x_1, \tag{4}$$

where x and y are x- and y-coordinates, respectively, and the subscript means the frame number of the microscope images. The direction of the x axis coincided with the direction in which the increase of the oxygen tension. After the three properties were measured, average speed (S_{avg}), persistence (P), directional persistence (DP), and chemotaxis index (CI) were quantified using the following equations:

$$S_{avg} = \frac{TPL}{T}, \tag{5}$$

$$P = \frac{ND}{TPL}, \tag{6}$$

$$DP = \frac{XDD}{TPL}, \tag{7}$$

$$CI = \cos\theta = \frac{XDD}{ND}. \tag{8}$$

G. Drug screening

Two anticancer agents, doxorubicin hydrochloride (DOX, Sigma-Aldrich) and tirapazamine (TPZ, Toronto Research Chemicals), were used. For both drugs, stock solutions were prepared with reference to the product protocols. The concentration of DOX was 0.01 μM, 0.1 μM, 1 μM, or 10 μM, and the concentration of TPZ was 10 μM, 50 μM, 100 μM, or 500 μM. In each case, the concentration was determined to cover the range of half-maximal inhibitory concentration (IC50).[32,33] The drug treatments were performed for three conditions with different oxygen tensions: hypoxia, gradient, and normoxia [Fig. S4(a) in the supplementary material]. Hypoxia condition was generated by supplying anoxic gas mixture at the both sides of the gas channel. For each condition, the experiment was run for 48 h, and the media in the media channels was replaced with fresh media 24 h after the experiment starts by introducing the drug-containing medium into the reservoirs of the medium channels. Then, the cancer cells were stained by calcein-AM and ethidium homodimer-1 (Invitrogen) to check cell viability. Finally, the viability of the cancer cells was quantified by dividing the number of live cells with the number of total cells.

H. Data analysis

Fluorescence intensity measurements and manual tracking of the cancer cell migration were measured using ImageJ (NIH). Significance comparisons between groups in all data were made using the unpaired Student's t-test. MATLAB R2019a

(MathWorks) was used for statistical analysis, and Origin Pro 2019 (OriginLab Corporation) was used for plotting.

III. RESULTS AND DISCUSSION

A. Oxygen tension distribution in the microfluidic device

The oxygen tension in the microfluidic device was calculated and measured in two ways through simulations and experiments. Figure 2(a) denotes the convergence curve of the oxygen tension in the middle of the gel (red dot) channel over time. As can be seen in the schematic, the measured point is set opposite to the direction in which the gas is flowing to ensure that the gas is sufficiently diffused. Besides, the oxygen tension was calculated according to the *Pe* number to determine the effect of oxygen tension on the flow rate of gas in the device [Figs. S1(a) and S1(b) in the supplementary material]. As shown in the graph, the difference in the oxygen tension due to the different gas flow rates corresponding to the four *Pe* numbers was not significant [Fig. S1(a) in the supplementary material]. And, Fig. S1(b) in the supplementary material shows the interface between coverslip and PDMS of the device, except for the case of $Pe = 1$, where the oxygen tension remained constant up to the outlet of the gas channel. Therefore, the flow rate of the gas corresponding to $Pe = 100$ was set so that a constant oxygen tension was maintained in the gas channel while the gas passed through the gas channels. As shown in Fig. 2(a), the oxygen tension has reached a nearly steady-state after about 60 min of transient state and about 90 min after the start time.

Then, the oxygen tension in the channels over time was calculated with the flow rate corresponding to $Pe = 100$ [Figs. S1(c) and S1(d) in the supplementary material]. The oxygen tension dropped rapidly before 60 min, and from then on, a stable gradient was formed [Fig. S1(c) in the supplementary material]. The enlarged graph in Fig. S1(c) in the supplementary material shows the oxygen tension at the time of 60, 90 min, and steady-state conditions in the gel channel section. After more than 60 min, the gradient has been formed almost identical to steady-state. It can be seen from Fig. S1(d) in the supplementary material that the gas has passed through the channel before 5 min and has reached a steady-state through diffusion inside the PDMS.

Based on the above results, the fluorescence images for the calculation of the oxygen tension in the experiment were obtained 90 min after the gas started flowing through the gas channels. As shown in the gray-scale image of Fig. 2(b), the oxygen tension was measured in the direction across the media–gel–media channel. Like the convergence curve in Fig. 2(a), the gas flow rate was adjusted to a sufficient velocity, $Pe = 100$, for both simulation and experiment to minimize the oxygen tension change in the gas channels during the gas flow. The green-colored region in the graph coincides with that of the gel channel. The results from simulation and experiment both showed that the oxygen tension in the gel channeled was between 10% and 17%.

B. Cellular response in different oxygen tension ranges

After the validation of the oxygen tension in the device, the response of the cancer cells under the oxygen tension gradient in the device was observed. The responses according to the different oxygen tension was confirmed by the immunostaining of the oxygen-specific marker, HIF-1α.[34]

Cells exposed to each condition for 24 h were immunostained [Fig. 3(a)], and fluorescent intensities of the nucleus and cytoplasm were measured under the same microscopic condition (Fig. S3 in the supplementary material). The mean fluorescence intensity of the nucleus increased 1.28-fold at the positive control with the addition of 100 μM $CoCl_2$ (25.8 ± 4.27) compared with that of the normoxic condition [20.2 ± 2.72; Fig. S3(a) in the supplementary material]. In the gradient conditions where the oxygen tensions range from 10% to 13.5% (left gradient) and 13.5% to 17% (right gradient), the average fluorescence intensities were 21.5 ± 2.68 and 22.3 ± 3.58, respectively, and were higher than normoxic condition. The mean fluorescence intensity of the cytoplasm was also showed a similar trend [Fig. S3(b) in the supplementary material]. The mean fluorescence intensity measured in the cytoplasm in the positive control was 21.2 ± 3.51, showing a significant difference when compared with the normoxic condition (19.1 ± 2.45, $p < 0.01$).

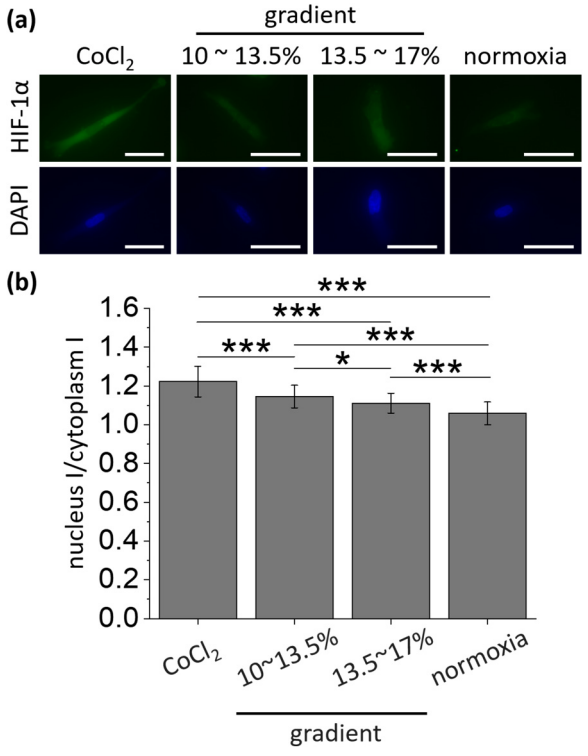

FIG. 3. Different cellular response to changes in oxygen tension. (a) Representative fluorescence images of HIF-1α (green) and DAPI (blue) corresponding to each condition. Scale bars = 50 μm. (b) The accumulation of HIF-1α (fluorescence intensity ratio) was observed highest in the positive control of hypoxia generated with $CoCl_2$ and lowest in normoxia. From positive control to normoxia in order from left, 127 cells (3 devices), 108 cells (4 devices), 107 cells (4 devices), and 122 cells (3 devices) were used. Error bars represent the standard error of the mean. $^{*}p < 0.05$ and $^{***}p < 0.001$.

However, there was no significant difference in the mean fluorescence intensity of the cytoplasm between the gradient conditions (18.8 ± 2.06 for left gradient condition and 20.1 ± 3.16 for right gradient condition) and the normoxic condition. Rather, there was a significant difference in the positive control and the left oxygen gradient condition, which is presumed to be influenced by device variations.

Subsequently, the ratio of fluorescence intensity between the nuclei and cytoplasm was calculated based on the fact that the frequency of HIF-1α translocation from cytoplasm to the nucleus increases under hypoxic condition with less degradation of HIF-1α in the cytoplasm [Fig. 3(b)].[34] The ratio of fluorescence intensity by staining of HIF-1α tended to rise with lower oxygen tension, and the mean value showed significant differences between oxygen conditions. The ratio of HIF-1α in the positive control (1.22 ± 0.079) was the highest, which was 15.1% higher than normoxic condition (1.06 ± 0.059). Two gradient conditions (1.15 ± 0.059 for left gradient condition and 1.11 ± 0.051 for right gradient condition) increased by 8.49% and 4.72%, respectively, compared to the normoxic condition, and had significant differences. Thus, we confirmed that the cells were sufficiently affected by the hypoxic stress in the device when the oxygen tension gradient was formed.

C. Biased cancer cell migration under oxygen tension gradient

Under an oxygen tension gradient, the motility and directionality of cancer cells were observed and quantified (Fig. 4). Migration behaviors of the cancer cells inside the fibrin gel were analyzed by setting the x axis coordinates in the direction with increasing oxygen tension as shown in Figs. 1(b) and 1(c).

It can be seen in Fig. 4(a) that the net displacement (*ND*) increased with decreasing oxygen tension. Under the normoxic condition, the *ND* averaged 50.1 μm, and 1st quartile (Q1) and 3rd quartile (Q3) of the lower and upper boundaries of the box plot were 29.2 μm and 67.5 μm, respectively. In the right gradient condition, the mean value of *ND* slightly increased to 52.7 μm and Q1 and Q3 of *ND* were 28.3 μm and 69.8 μm, respectively, with no significant difference. However, in the left gradient condition, the mean *ND* was 55 μm, Q1 was 31.2 μm, and Q3 was 74.7 μm, which were significantly increased compared to normoxic condition. The measured *TPL* in Fig. 4(b) also showed a tendency to increase as the oxygen tension decreased. In each right and left gradient condition, the mean total path length (*TPL*) increased by 1.11-fold and 1.13-fold compared to the normoxic condition. This was confirmed to have the similar results as that of the previous research.[26] The x-directional displacement (*XDD*) of the cancer cells in the same direction as the oxygen tension gradient showed slightly different but not significant results. In Fig. 4(c), in normoxic condition, the mean *XDD* was −0.49 μm, whereas in right and left gradient conditions, the *XDD* averaged 1.69 μm and 2.44 μm, respectively.

In the context of *ND* and *TPL*, the average speed S_{avg} also increased with decreasing oxygen tension [Fig. 4(d)]. In normoxic condition, the S_{avg} of cancer cells had the mean of 13.4 μm/h, Q1 of 8.68 μm/h, and Q3 of 16.4 μm/h. In the right gradient condition, the mean S_{avg} increased to 14.8 μm/h, which is 1.1-fold higher than that of normoxic condition. Q1 and Q3 also increased to 9.51 μm/h and 19 μm/h, respectively, compared to normoxic condition. The S_{avg} of the left gradient condition showed a more marked difference, the mean S_{avg} is 15.1 μm/h, which is 1.13-fold higher than normoxic condition, and Q1 and Q3 of S_{avg} are 10.3 μm/h and 19.4 μm/h, respectively, which increased 1.19-fold and 1.18-fold than those of normoxic condition. This is a result of the same context as the previous studies that hypoxia stimulates the invasion of cancer cells.[35] The modulation of Rab11 through the stabilization of microtubules regulates integrin α6 trafficking could be one of several factors that affect the cancer cell migration. In addition to the factors caused inside the cancer cells, the effects of the factors outside of the cancer cells can be considered. Another presumable factor, ECM remodeling, which can be caused by hypoxia makes the ECM stiff and aligned than in normoxia.[36] Since the invasiveness of the cancer cells can be increased within the stiff and aligned ECM,[37] it can be inferred that cancer cells may have a higher S_{avg} at lower oxygen tension.

Following the motility of the cancer cells, the directionality was quantified [Figs. 4(e) and 4(f)]. The persistence P under all three conditions showed similar trends, and under the right and left gradient conditions, the mean values of P had no significant differences compared to the normoxic condition [Fig. 4(e)]. On the other hand, the directional persistence *DP* in the right gradient and left gradient increased by 2.27-fold and 9.7-fold compared to the absolute mean value of *DP* in normoxic condition, showing a significant increase in the left gradient condition compared to normoxic condition [Fig. 4(f)]. The cancer cells tended to migrate in the direction of higher oxygen tension, which was enhanced in lower oxygen tension ranges, suggesting that oxygen plays an important role in cancer metastasis. When compared to the previous study where the cells showed directionality toward low oxygen tension, the results are somewhat inconsistent. This was speculated due to the effect of rheotaxis by the flow from upstream to downstream[44] and the structure of the device used in this study, which induced compensatory action by nutrient supply from medium channels at both ends of the oxygen tension gradient which has a similar structure to the previous research.[47] The chemotaxis index *CI* also indicated this migratory tendency though no significant difference was confirmed between the oxygen conditions [Fig. 4(g)]. The densely clustered tumor and poor vascularization trigger a poor supply of oxygen including other nutrient supply.[38] Therefore, the cancer cells may tend to move in the direction of higher oxygen tension by a mechanism inside the cancer cells to solve this problem. As a preliminary study to support the directionality of the cells for the oxygen and nutrient supply, Mosadegh *et al.* showed the directional migration of the cancer cells when oxygen was supplied in one direction using a stacked paper-based invasion assay. Moreover, the cancer cells had enhanced directionality in the condition where nutrients were not supplied as well as oxygen.[45]

The tumor microenvironment with poor oxygen supply leads to chronic or transient hypoxia, which changes the characteristics and the physiologies of the cancer cells including motility and drug resistance through oxygen-specific marker, HIF.[7,8] The changes in the motility of cancer cells by the HIF pathway can be found not

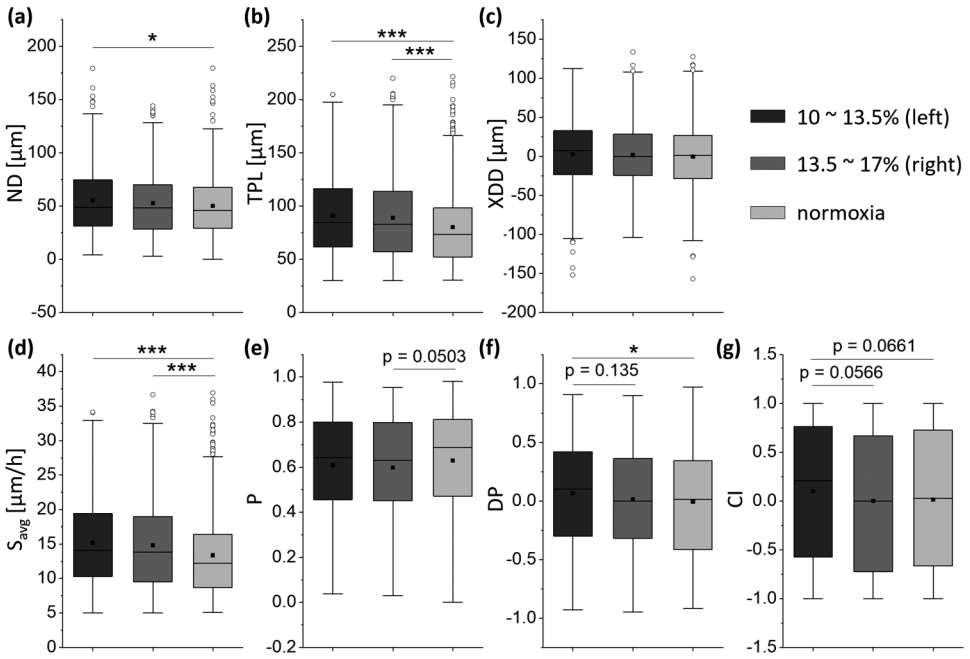

FIG. 4. Motility and directionality affected by oxygen tension. (a) The net displacement, *ND*. For 6 h, the cancer cells had greater *ND* under gradient conditions and the trend increased with lower oxygen levels. (b) The total path length, *TPL*. Like (a), *TPL* also had a higher value when the oxygen tension gradient was formed, and the tendency was larger at lower oxygen tension. (c) The *x*-directional displacement, *XDD*. Under gradient conditions, cancer cells showed a small tendency to move toward higher oxygen levels. (d) The average speed, S_{avg}. The cancer cells had higher S_{avg} at lower oxygen tensions. (e) The persistence, *P*. The cancer cells showed similar values of *P* regardless of differences in oxygen tension. (f) The directional displacement, *DP*. Under the oxygen tension gradient, the cancer cells tended to migrate in the direction of higher oxygen tension, and this tendency was more enhanced in the low oxygen tension range. (g) Chemotaxis index, *CI*. Although the cancer cells tended to migrate toward the higher oxygen tension side in the low oxygen tension range, *CI* did not show any significant difference as in *DP*. For left gradient, right gradient and normoxia in order from left, 391 cells (7 devices), 334 cells (7 devices), and 590 cells (10 devices) were analyzed. The lower and upper boundaries of each box represent 1st quartile (Q1) and 3rd quartile (Q3), respectively, and the whisker ranges from minimum to maximum, where the minimum and maximum are Q1 minus 1.5 times the box's interquartile range and Q3 plus 1.5 times the interquartile range, respectively. The horizontal line and the rectangular dot in each box are the median and the mean, respectively, and the circular points outside the whisker is the outliers. $^{*}p < 0.05$, $^{**}p < 0.01$, and $^{***}p < 0.001$.

only in the constant hypoxic environment but also in the periodic hypoxic environment.[9] In both cases, the cancer cells are more invasive in a hypoxic environment, resulting in a higher probability of cancer metastasis.[39] One of the several downstream events of the HIF pathway that causes increased migration and metastasis of breast cancer cells in a hypoxic environment can be associated with decreased epithelial cadherin (E-cadherin) via Notch signaling.[10] In addition to the casual relationship caused by the HIF pathway, another pathway caused by the hypoxic environment also upregulates the migration of cancer cells.[11] Consistently, the hypoxic environment affects the activity of cancer cells in an increasing direction. Furthermore, it was reported that the cells migrated toward the lower pH when extracellular pH was not uniform.[40] Considering the lowering of the extracellular pH due to glycolysis in hypoxia,[41] this may be considered as one of the factors that prevented the distinct directionality of the cancer cells due to the difference in the oxygen tension. It is expected that the relationship among the oxygen tension, cancer cell motility and directionality will be clearer in the future by expanding and adjusting the range of oxygen tension.

D. Oxygen-dependent cancer cell viability under anticancer drug

In the tumor microenvironment, which is locally hypoxic, some anticancer drugs are affected by the oxygen tension.[7] Therefore, as another application of the microfluidic device in which the oxygen tension was controlled, the anticancer efficacy was compared (Fig. 5). The oxygen tensions were calculated in the microfluidic device for uniform hypoxia, gradient, and normoxia conditions [Fig. S4(a) in the supplementary material]. The different ranges of oxygen tension were generated in the gel channel, where cancer cells were introduced. The viability of the cancer cells in the microfluidic device for 48 h was first checked using a drug-free culture medium and the results showed no significant differences in viability due to oxygen tension [Fig. S4(b) in the supplementary material].

Two anticancer drugs, TPZ and DOX, were then applied to the cancer cells to compare the efficacy of anticancer drugs according to the difference in the oxygen conditions. In the case of TPZ, the viability of the cancer cells varied significantly as the oxygen tension decreased

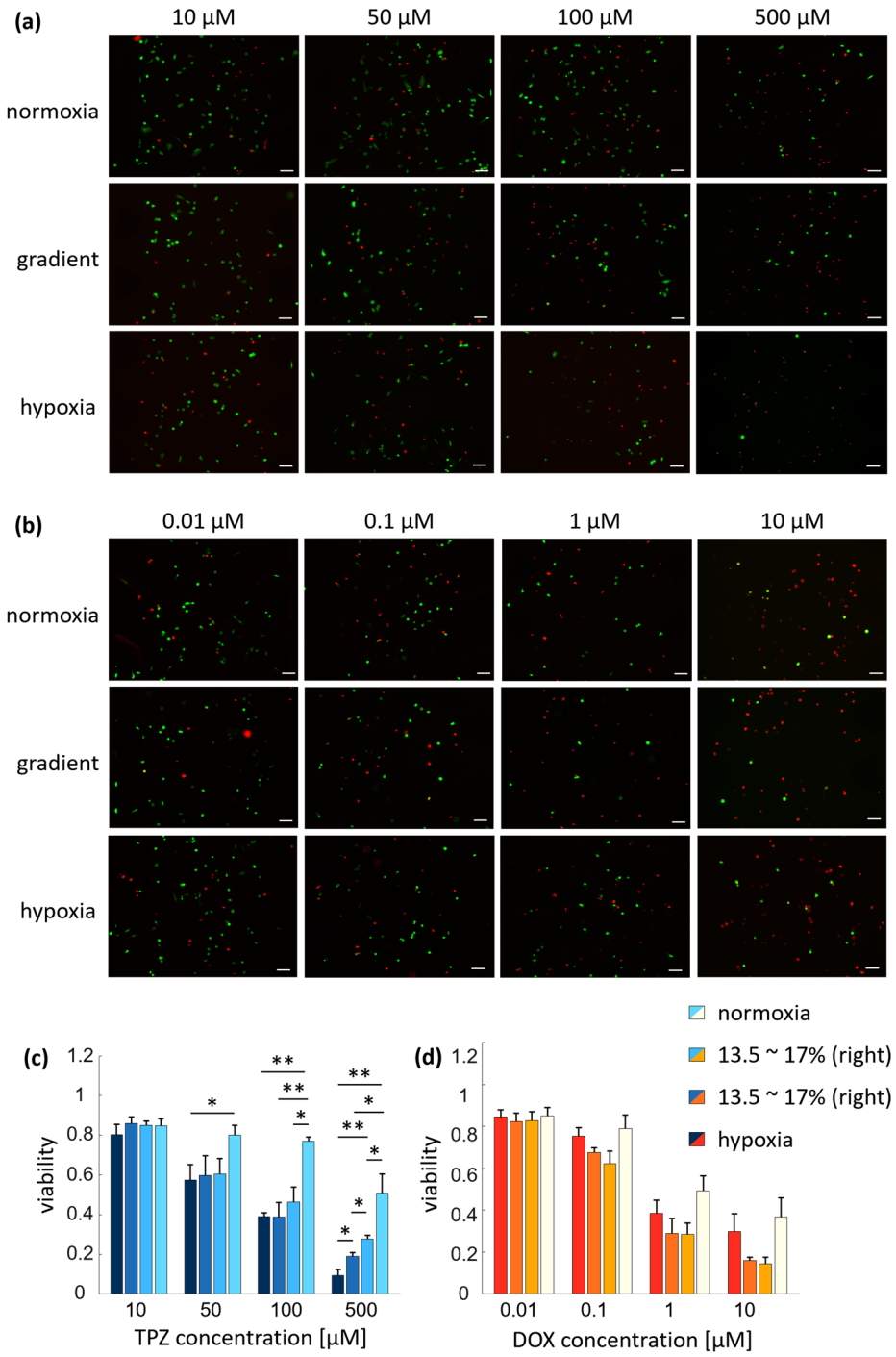

FIG. 5. Anticancer efficacy under various oxygen levels. (a) Representative live/dead micrographs different oxygen tensions and TPZ concentrations. (b) Representative live/dead micrographs with different oxygen tensions and DOX concentration. (c) Viability of the cancer cells for different TPZ concentration and oxygen tensions. As the concentration of TPZ increased, the viability was greatly affected by oxygen tension. In particular, at 500 μM, the viability of the cancer cells was significantly different due to the difference in oxygen tensions. The lower the oxygen tension, the lower the viability of the cancer cells. (d) Viability of the cancer cells for different DOX concentrations and oxygen tensions. Cancer cells were not significantly affected by oxygen tension at the same DOX concentration. Although not significant, the viabilities were lower in the gradient conditions than in other conditions. For each condition, three devices were used. Scale bars = 100 μm. Error bars represent the standard error of the mean (n = 3). *$p < 0.05$ and **$p < 0.01$.

and as the drug concentration increased [Figs. 5(a) and 5(c)]. When the concentration of TPZ was 10 μM, the viability of the cancer cells was not significantly affected by oxygen tension (0.8 ± 0.052, 0.85 ± 0.022, 0.85 ± 0.033, and 0.85 ± 0.034 for hypoxia, left gradient, right gradient, and normoxia, respectively). It seems that the concentration of TPZ was low to result in any significant. However, when the concentration of the drug was increased to 50 μM, the efficacy of TPZ was enhanced in the hypoxia and gradient conditions, showing the viability of the cancer cells of 0.57 ± 0.079, 0.6 ± 0.098, and 0.6 ± 0.79, respectively, compared to normoxia under which the

viability of the cancer cells was 0.8 ± 0.05. With further increased concentration of the drug at 100 μM, the viability of the cancer cells in hypoxia and gradient conditions decreased steadily to 0.36 ± 0.021, 0.39 ± 0.073, and 0.46 ± 0.075, respectively, whereas in normoxia, the decrease was relatively small (0.77 ± 0.022). Finally, at 500 μM, the viability decreased by 88.38% in hypoxia to 0.093 ± 0.029 compared to 10 μM, whereas in gradient conditions, the viabilities were 0.19 ± 0.018 and 0.28 ± 0.02, which were reduced by 77.91% and 67.59% compared to 10 μM. Under normoxia, the viability was 0.51 ± 0.097, which was 40% decrease compared to 10 μM. This trend of enhanced response of the cancer cells to TPZ under the hypoxic condition is similar to previous research in which the viabilities of cancer cells treated with 100 μM TPZ under hypoxic conditions of approximately 1.7%–3.8% oxygen tensions ranged from 0.05 to 0.35.[12,13,32,44] The slight variation of the viability values may be due to the difference in the range of oxygen tension or by the difference in the cell lines used. Comprehensively, through the previous studies and the above results, it was confirmed that the efficacy of TPZ, which is activated at low oxygen tension, increased at lower oxygen levels.

The results with DOX under the same oxygen conditions led to different trends than those with TPZ [Figs. 5(b) and 5(d)]. Although the viability of the cancer cells decreased as the concentration of DOX increased, as in the case of TPZ, the viability did not decrease as the oxygen tension decreased [Fig. 5(d)]. However, there was a small tendency of lower viability in the oxygen gradient conditions and it is noteworthy that the gradient conditions were neither the lowest nor the highest oxygen level condition. The viability of cancer cells at the lowest DOX concentration of 0.01 μM was similar in hypoxia, gradient, and normoxia, 0.85 ± 0.033, 0.82 ± 0.042, 0.83 ± 0.043, and 0.85 ± 0.041, respectively. However, as the drug concentration increased to 0.1 μM, the viability was 0.75 ± 0.04 and 0.79 ± 0.065 in hypoxia and normoxia, respectively, while the viability dropped in the gradient conditions (0.67 ± 0.023 and 0.62 ± 0.061). Although not significant, the same tendencies of lowest viability under gradient conditions were found when DOX was applied at 1 μM and 10 μM (viability from hypoxia, gradient to normoxia, 0.39 ± 0.062, 0.28 ± 0.073, 0.28 ± 0.054, and 0.49 ± 0.071 for 1 μM; 0.3 ± 0.085, 0.16 ± 0.015, 0.14 ± 0.03, and 0.37 ± 0.092 for 10 μM). This tendency of the lowest viability in the oxygen gradient conditions may be due to the combination of different effects of DOX depending on the oxygen level. In hypoxic tumor microenvironment, the cancer cells cannot receive enough oxygen for metabolism from the outside. Then, the breast cancer cells need to obtain the energy required through glycolysis, which lowers the internal and external pH of the cell due to the byproducts.[41] The low pH leads to increase in the ionization of weak bases, whereas drugs usually pass through the cell membrane in an uncharged state.[28] Taken together, the weak base DOX may have relatively less efficacy in low pH conditions.[7] For example, Born *et al.* showed that the decreased uptake of DOX when the pH was lowered.[46] On the other hand, DOX may also has the characteristic of increasing its efficacy in hypoxia because it functions to prevent HIF-1α from binding to DNA.[6] Thus, it suggests that there may be conditions under which DOX will have the best efficacy in the specific oxygen tension range by competing for the positive and negative effects of oxygen.

The results of the anticancer drug screening in different oxygen levels by TPZ and DOX suggest that the dosage of some anticancer drugs should be considered and adjusted accordingly to the exposed hypoxic microenvironment. This is also in line with the recent interests in HIF, which has increased expression in the hypoxic milieu, as a major target of anticancer drugs.[42,43]

IV. CONCLUSIONS

We employed a microfluidic device composed of oxygen-permeable PDMS to mimic the oxygen tension gradient in the tumor microenvironment and confirmed its feasibility through the cell response and various applications according to different oxygen levels. As the results, it was confirmed that the cancer cells prefer to migrate toward the higher oxygen tension side, implying the oxygen tension gradient may affect the cancer metastasis in the body. Also, the necessity of adjusting the concentration of the drug according to the oxygen tension was raised. Further research on the directionality of the cancer cells and drug screenings concerning locally hypoxic tumor environment will give us deeper insight.

SUPPLEMENTARY MATERIAL

See the supplementary material for (1) detailed estimation of the oxygen tension in the microfluidic device, (2) fluorescent intensities of HIF-1α in nucleus and cytoplasm, and (3) estimation of the oxygen tension for drug screenings and viability in control.

ACKNOWLEDGMENTS

The authors would like to thank Seunggyu Kim for helpful discussion of selecting research topics. This work was supported by the Basic Science Research Program (2017R1D1A1B03030428) through the National Research Foundation of Korea (NRF) funded by the Ministry of Education and by the KAI-NEET Institute of KAIST (N11200049). K.F. acknowledges JSPS KAKENHI (Grant No. 16H05906).

DATA AVAILABILITY

The data that support the findings of this study are available within the article and its supplementary material.

REFERENCES

[1]G. Disibio and S. W. French, Arch. Pathol. Lab. Med. **132**(6), 931–939 (2008).
[2]A. B. Mariotto, K. Robin Yabroff, Y. Shao, E. J. Feuer, and M. L. Brown, J. Natl. Cancer Inst. **103**(2), 117–128 (2011).
[3]A. Mullard, Nat. Rev. Drug Discovery **15**(5), 299 (2016).
[4]B. J. Vakoc, R. M. Lanning, J. A. Tyrrell, T. P. Padera, L. A. Bartlett, T. Stylianopoulos, L. L. Munn, G. J. Tearney, D. Fukumura, and R. K. Jain, Nat. Med. **15**(10), 1219–1223 (2009).
[5]F. R. Balkwill, M. Capasso, and T. Hagemann, J. Cell Sci. **125**(23), 5591–5596 (2012).
[6]X. Lu and Y. Kang, Clin. Cancer Res. **16**(24), 5928–5935 (2010).
[7]I. F. Tannock, Cancer Metastasis Rev. **20**(1–2), 123–132 (2001).
[8]V. Petrova, M. Annicchiarico-Petruzzelli, G. Melino, and I. Amelio, Oncogenesis **7**(1), 1–13 (2018).
[9]R. A. Cairns, T. Kalliomaki, and R. P. Hill, Cancer Res. **61**(24), 8903–8908 (2001).
[10]J. Chen, N. Imanaka, and J. Griffin, Br. J. Cancer **102**(2), 351–360 (2010).

[11]A. Nagelkerke, J. Bussink, H. Mujcic, B. G. Wouters, S. Lehmann, F. C. Sweep, and P. N. Span, Breast Cancer Res. **15**(1), R2 (2013).
[12]Z. Wang, Z. Liu, L. Li, and Q. Liang, Microfluid. Nanofluid. **19**(6), 1271–1279 (2015).
[13]L. Wang, W. Liu, Y. Wang, J.-C. Wang, Q. Tu, R. Liu, and J. Wang, Lab Chip **13**(4), 695–705 (2013).
[14]W. J. Polacheck, J. L. Charest, and R. D. Kamm, Proc. Natl. Acad. Sci. U.S.A. **108**(27), 11115–11120 (2011).
[15]S. Lim, H. Nam, and J. S. Jeon, Biophys. J. **115**(10), 2034–2043 (2018).
[16]J. T. Price, T. Tiganis, A. Agarwal, D. Djakiew, and E. W. Thompson, Cancer Res. **59**(21), 5475–5478 (1999).
[17]L. Gómez-Cuadrado, N. Tracey, R. Ma, B. Qian, and V. G. Brunton, Dis. Models Mech. **10**(9), 1061–1074 (2017).
[18]N. E. Sharpless and R. A. DePinho, Nat. Rev. Drug Discovery **5**(9), 741–754 (2006).
[19]B. M. Baker and C. S. Chen, J. Cell Sci. **125**(13), 3015–3024 (2012).
[20]Y. Imamura, T. Mukohara, Y. Shimono, Y. Funakoshi, N. Chayahara, M. Toyoda, N. Kiyota, S. Takao, S. Kono, and T. Nakatsura, Oncol. Rep. **33**(4), 1837–1843 (2015).
[21]A. M. Ghaemmaghami, M. J. Hancock, H. Harrington, H. Kaji, and A. Khademhosseini, Drug Discovery Today **17**(3–4), 173–181 (2012).
[22]A. G. Toh, Z. Wang, C. Yang, and N.-T. Nguyen, Microfluid. Nanofluid. **16**(1–2), 1–18 (2014).
[23]M. B. Byrne, M. T. Leslie, H. R. Gaskins, and P. J. Kenis, Trends Biotechnol. **32**(11), 556–563 (2014).
[24]M. Adler, M. Polinkovsky, E. Gutierrez, and A. Groisman, Lab Chip **10**(3), 388–391 (2010).
[25]M. Polinkovsky, E. Gutierrez, A. Levchenko, and A. Groisman, Lab Chip **9**(8), 1073–1084 (2009).
[26]K. Funamoto, I. K. Zervantonakis, Y. Liu, C. J. Ochs, C. Kim, and R. D. Kamm, Lab Chip **12**(22), 4855–4863 (2012).
[27]M. L. Rexius-Hall, G. Mauleon, A. B. Malik, J. Rehman, and D. T. Eddington, Lab Chip **14**(24), 4688–4695 (2014).
[28]G. Helmlinger, F. Yuan, M. Dellian, and R. K. Jain, Nat. Med. **3**(2), 177–182 (1997).
[29]D. Yoshino and K. Funamoto, AIP Adv. **9**(4), 045215 (2019).
[30]Y.-A. Chen, A. D. King, H.-C. Shih, C.-C. Peng, C.-Y. Wu, W.-H. Liao, and Y.-C. Tung, Lab Chip **11**(21), 3626–3633 (2011).
[31]G. Wang, T. K. Hazra, S. Mitra, H.-M. Lee, and E. W. Englander, Nucleic Acids Res. **28**(10), 2135–2140 (2000).
[32]C.-C. Peng, W.-H. Liao, Y.-H. Chen, C.-Y. Wu, and Y.-C. Tung, Lab Chip **13**(16), 3239–3245 (2013).
[33]L. Smith, M. B. Watson, S. L. O'Kane, P. J. Drew, M. J. Lind, and L. Cawkwell, Mol. Cancer Ther. **5**(8), 2115–2120 (2006).
[34]M. C. Brahimi-Horn and J. Pouysségur, J. Cell Sci. **122**(8), 1055–1057 (2009).
[35]S.-O. Yoon, S. Shin, and A. M. Mercurio, Cancer Res. **65**(7), 2761–2769 (2005).
[36]D. M. Gilkes, S. Bajpai, P. Chaturvedi, D. Wirtz, and G. L. Semenza, J. Biol. Chem. **288**(15), 10819–10829 (2013).
[37]M. H. Zaman, L. M. Trapani, A. L. Sieminski, D. MacKellar, H. Gong, R. D. Kamm, A. Wells, D. A. Lauffenburger, and P. Matsudaira, Proc. Natl. Acad. Sci. U.S.A. **103**(29), 10889–10894 (2006).
[38]P. Vaupel, F. Kallinowski, and P. Okunieff, Cancer Res. **49**(23), 6449–6465 (1989).
[39]S. M. Ehsan, K. M. Welch-Reardon, M. L. Waterman, C. C. Hughes, and S. C. George, Integr. Biol. **6**(6), 603–610 (2014).
[40]R. K. Paradise, M. J. Whitfield, D. A. Lauffenburger, and K. J. Van Vliet, Exp. Cell Res. **319**(4), 487–497 (2013).
[41]J. Pouysségur, F. Dayan, and N. M. Mazure, Nature **441**(7092), 437–443 (2006).
[42]S. J. Welsh and G. Powis, Curr. Cancer Drug Targets **3**(6), 391–405 (2003).
[43]A. Giaccia, B. G. Siim, and R. S. Johnson, Nat. Rev. Drug Discovery **2**(10), 803–811 (2003).
[44]C.-W. Chang, Y.-J. Cheng, M. Tu, Y.-H. Chen, C.-C. Peng, W.-H. Liao, and Y.-C. Tung, Lab Chip **14**(19), 3762–3772 (2014).
[45]B. Mosadegh, M. R. Lockett, K. T. Minn, K. A. Simon, K. Gilbert, S. Hillier, D. Newsome, H. Li, A. B. Hall, and D. M. Boucher, Biomaterials **52**, 262–271 (2015).
[46]R. Born and H. Eichholtz-Wirth, Br. J. Cancer **44**(2), 241–246 (1981).
[47]R. Koens, Y. Tabata, J. C. Serrano, S. Aratake, D. Yoshino, R. D. Kamm, and K. Funamoto, APL BioEng. **4**(1), 016106 (2020).